Heliyon 9 (2023) e18483

Contents lists available at ScienceDirect

Heliyon

journal homepage: www.cell.com/heliyon

Effect of tip winglet position on tip flow and noise of axial flow fan

Lei Diao [a,*], Fahua Ge [a], Yong Liu [a], Lin Yang [a], Youen Liu [a], Qi Huang [b]

[a] Guizhou Aerospace Linquan Motor Co.,Ltd, Guiyang, Guizhou, 550081, China
[b] Guizhou University, Guiyang, Guizhou, 550025, China

ARTICLE INFO

Keywords:
Axial flow fan
Tip winglet
Internal flow characteristic
Fan noise
Tip leakage flow

ABSTRACT

In order to investigate the impact of blade tip winglet position on the internal flow and noise characteristics of axial flow fans,three different blade tip winglets,namely the TSW blade, the SSW blade, and the PSW blade,were hereby proposed. The accuracy of the simulation model was verified through experiments, and the circumferential internal flow characteristics and noise characteristics of these different blades were studied by numerical simulation using the blade tip partition method. The calculation results indicated the high-level efficiency of TSW, SSW and PSW blades in reducing the blade tip leakage flow in Z1 and Z2 regions and suppressing its circumferential propagation in the Z3 region. Besides, it was found that SSW blade and PSW blade had larger total pressure loss relative to Ori blade, and that TSW had higher total pressure difference at low blade height. Additionally TSW blades performed the best in improving the blade tip blockage,while TSW, SSW and PSW blades effectively reduced the leakage flow against the main stream, and blade tip winglet blades could effectively improve the fan discrete noise, SSW had the most significant noise reduction effect in the total sound pressure level, and in the overall blade,Z1, Z2 and Z3 were reduced by 2.16 dB,1.68 dB,2.24 dB and 3.74 dB.

1. Introduction

As the system equipment performance requirements perpetually advance, demands on auxiliary fans are correspondingly rising. The flow within the blade tip gap of the fan embodies significant inconsistencies and complexities. The secondary flow, also known as the tip leakage vortex, stands as the principal contributor to fan loss and blockage, affecting the stability of the fan. The intense vortex noise produced by the blade tip gap comprises a critical component of the overall pneumatic noise. Thus, controlling the blade tip leakage flow makes it possible to enhance the pneumatic noise of the fan. Therefore, it has been proven efficient to ameliorate the performance and noise of the fan by unveiling the flow characteristics in the tip clearance and regulating the flow state of the tip leakage. Techniques such as blade tip reshaping, magazine treatment, suction, blowing treatment, plasma discharge, and blade tip winglet technology are prevalently implemented as active and passive measures for controlling blade tip leakage flow.Numerous studies have been carried out by many scholars for the blade tip leakage flow control methods and aerodynamic noise reduction.A.For instance, Maaloum et al. [1] found the important noise sources corresponding to the high pressure fluctuation region located at the blade tip using potential flow methods; Jung,J.H [2] analyzed the flow structure at the blade tip due to the position of the winglets and confirmed the existence of an optimal blade tip clearance. Hoeger [3] pointed out the existence of peak blockages in the channel based

* Corresponding author.
E-mail addresses: diaolei0@126.com (L. Diao), gefahua@163.com (F. Ge), 12401593@qq.com (Y. Liu), 1425258582@qq.com (L. Yang), 1764852555@qq.com (Y. Liu), snk@163.com (Q. Huang).

https://doi.org/10.1016/j.heliyon.2023.e18483
Received 23 March 2023; Received in revised form 27 May 2023; Accepted 19 July 2023
Available online 23 July 2023

Nomenclature

Z	Number of blades
n	Rotational Speed
h	Hub ratio
e	Tip clearance
T	Blade thickness
C	Tip chord length
Ki	Impeller axial width
Kc	Axial width of fan casing
Δp	Total differential pressure
Cp	Time-averaged pressure coefficient
Cn	Dense flow gradient
b	Blockage coefficient
μ	Axial momentum
Hr	Relative helicity

on numerical simulation results of a large number of transonic compressor rotors and blade grilles,whose distribution characteristics were clearly influenced by the interaction of leakage vortices and excitation waves. Liu B [4] quantitatively analyzed the characteristics of the blockage distribution in the rotor channel under different measurement conditions, and the blade tip leakage blockage showed nonlinear and nonmonotonic characteristics. Han,S [5] found that the geometric arrangement of the winglets could change the trajectory of tip leakage vortices; Bizjan et al. [6] found that the tip winglets could effectively convert pressure into flow kinetic energy while reducing the emitted noise level. Erik W. Schneehagen [7] conducted an experimental study of aerodynamic acoustic noise reduction with three different end plate geometriesand found that the application of end plates changed the tip vorticity and reduced the aerodynamic acoustic noise contribution of the tip Nashimoto [8] measured the aerodynamic noise and wake velocity distribution and found from flow visualization and PIV measurements that the effect of winglets appeared in the traces of vorticity at the tip of the blade, the vorticity in the near wake region decreased and the aerodynamic noise decreased. Milavec,M and Yang Wei et al. [9,10] analyzed different rotor blade tip shapes, and the airflow in the tip gap of different blade tip shapes, confirming that dynamics of the airflow in the tip gap of different tip shapes were significantly different and played a key role in the generation and magnitude of the total noise.

Most preceding research has primarily analyzed the overall aerodynamic and noise conditions of axial fans, featuring a conspicuous absence of segmented studies and related quantitative analysis of blade tip conditions. To fill this gap, aiming to focus the research on blade tip nuances, three types of tip winglet blades, i.e., the TSW blade, the SSW blade, and the PSW blade, were hereby proposed. By employing blade tip partition modeling, the internal flow characteristics and noise profiles of the different blade tips were examined, followed by a parallel quantitative analysis. A preliminary exploration of the impact of adding a winglet surface to the blade tip on the internal flow and acoustic performance of the axial flow fan blade was conducted. Overall, the present study could potentially aid in optimizing the performance of axial flow fan engineering products.

2. Research subjects and methods

2.1. Research subjects

A small axial fan designed with a maximum static pressure of 680 Pa and an outlet flow rate of 440 m^2/h was chosen as the study object, and its basic parameters are shown in Table 1. For the convenience of calculation, the armature and magnet were replaced with cylindrical entities, and the outlet fence and other details were disregarded. Besides, details such as the chamfering of the prototype fan blade were reconstructed to ensure the convergence of the calculation, and the axial fan model is shown in Fig. 1.

In order to study the influence of the blade tip winglet adding position on the fan blade tip internal flow and noise characteristics,

Table 1
Transitions selected for thermometry.

Parameters	Numerical value
Z	5
n,r/min	8400
h	0.556
e,mm	2
T,mm	1.5–2.5
C,mm	47.66
Ki,mm	23.8
Kc,mm	38.0

three blade tip winglet adding modes were proposed based on the original airfoil type (Ori blade), as shown in Fig. 2, adding blade tip winglet, (SSW blade) on the suction side,adding blade tip winglet (PSW blade) on the pressure side, and adding blade tip winglet (TSW blade) on both sides of the suction and pressure sides of the blade at the same time. Blade inclination angle were set to be 0°; wing width, 1 mm; and wing height, 1.3 mm.

2.2. Numerical simulation methods and experimental validation

To refine the study of the blade tip winglet, the rotational domain was divided into three regions,i.e.,Z1, Z2 and Z3, and the blade tip winglet were in the Z1 and Z2 regions. The numerical model extended the inlet and outlet to 250 mm and 500 mm to avoid the influence of backflow on the calculation results. The interfacial connection was adopted,.The import and export domain was divided by structured grid, the rotating domain was divided by unstructured grid, and the impeller wall surface was grid encrypted. Besides the grid number of the impeller area was about 2.12 million, and the total grid number was 2.83 million. The turbulence model was selected as the k-e Realizable turbulence model, and the inlet and outlet pressures were set to a standard atmosphere. The rotational domain speed was set to be 8400r/min, and the MRF method was used for the constant calculation,while the slip grid is used for the non-constant calculation. The control equations were Navier-Stokes equations,solved by SIMPLEC method. The pressure correction was in a Standard way, and the spatial discrete format of momentum equation,turbulent kinetic energy equation and dissipation equation was in second order windward format. The residuals of the monitored outlet air volume values in the constant calculation were considered to be converged in the case of values less than 10^{-4}. After the convergence of the constant flow field calculation, the results of the constant flow field calculation were used as the initial flow field for the non-constant calculation.

The highest frequency that could be captured by the Fourier transform was related to the non-constant time step by the following equation.

$$\Delta t = \frac{f}{2} \tag{1}$$

Considering the calculation volume, the calculation frequency of numerical calculation was chosen as 1×10^4 Hz within the audible range of human ear, and the calculated fan rotated steadily for 10 weeks,with a total time duration of 7.14×10^{-2},a set step size of 5×10^{-5},a total step number of 1428, and an iteration step number of 20,respectively.After the non-constant calculated fan rotated for 10 weeks, the acoustic flow field was in a stable state, and the calculated results were used as the initial flow field for the large vortex simulation. The subgrid model was used for the simulation, and the dynamic stress model is selected. The FW-H equation in the open acoustic analog theory solved the near-field information to obtain the blade surface pressure pulse, and the sound pressure was further obtained by fast Fourier transform. The noise reflection between the fan casing and the impeller,etc. was ignored in the calculation process, and the noise receiving point was set at 1 m of the fan inlet and outlet. Fan wind tunnel experiment site is shown in Fig. 3. The fan sealed and fixed in the wind tunnel inlet, the test bench built-in auxiliary fan, start auxiliary fan and the fan under test, wind tunnel test bench connected to the data acquisition platform, by adjusting the size of the wind tunnel, the fan for wind tunnel experiments. As shown in Fig. 4, the results of the steady-state flow field were calculated to plot the fan P-Q curve and compare the experimental results, the flow rate and static pressure errors were less than 5%.

This section has been adjusted to improve the logical coherence of the statements.

As shown in Fig. 5, the A-weighted total sound pressure level noise test was conducted in the anechoic chamber for the fan under test, and the fan under test was one meter away from the tester. The test result was 52.4 dB, with an error of 3.1% compared to the numerical calculation.

Therefore, this indicates that the numerical simulation method used in this study is highly reliable and adequately ensures the accuracy of the subsequent analysis.

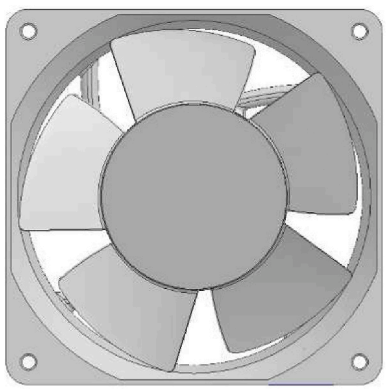

Fig. 1. Axial fan model drawing.

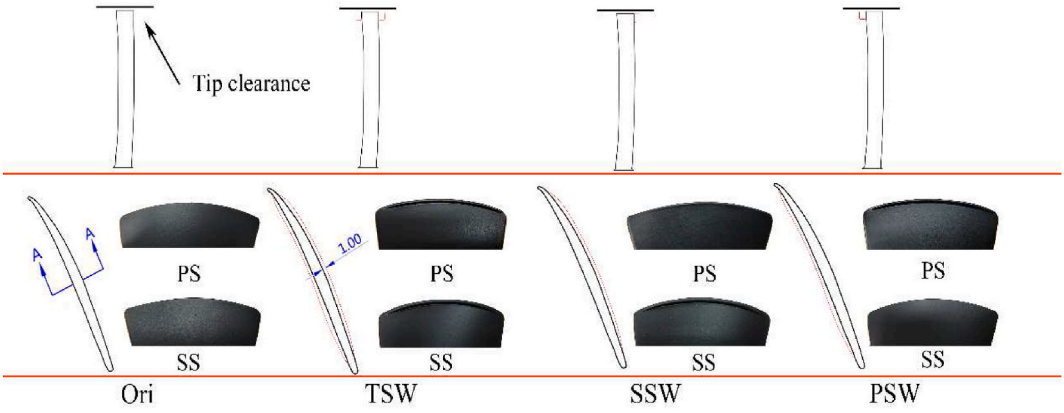

Fig. 2. Blade tip winglet configuration scheme.

Fig. 3. Wind tunnel experiment site.

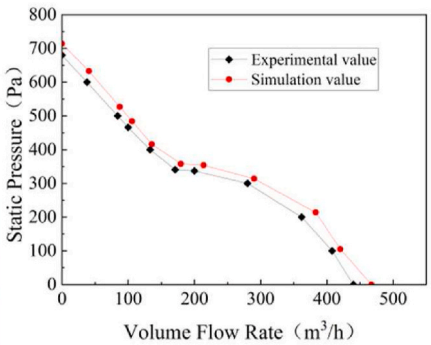

Fig. 4. P–Q curve comparison.

3. Results and analysis

3.1. Analysis of the flow field inside the circumferential blade tip

The time-averaged pressure coefficient equation is as follows.

$$c_p = \frac{(p_s - p_{s,inlet})}{\frac{1}{2}\rho u^2} \tag{2}$$

where, p_s is the local static pressure; $p_{s,inlet}$, the average static pressure at the inlet; ρ, the density; and u, the rotor 50% tangential velocity degree.

Fig. 6 depicts the contour plots of the time-averaged pressure coefficient at 40% of the blade height for different blade tip winglets

Fig. 5. Noise test site.

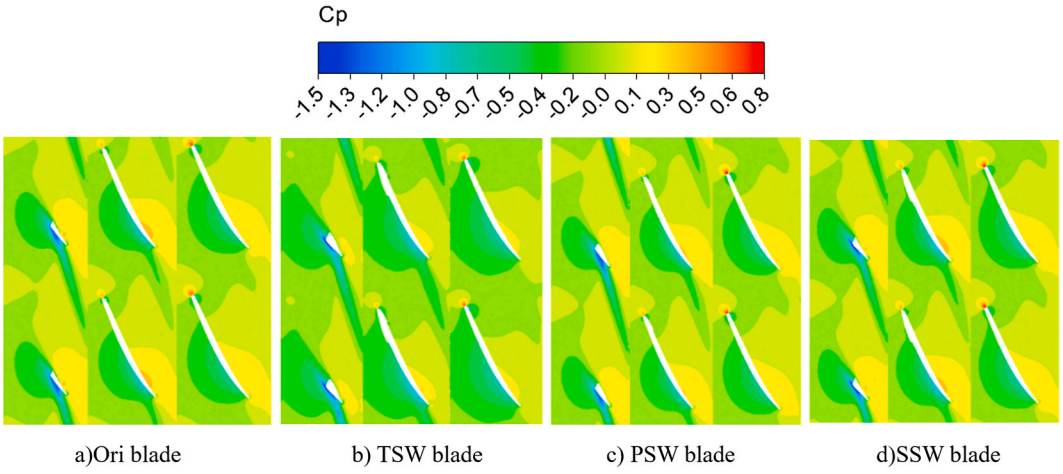

Fig. 6. Time-averaged pressure coefficients for different blade tip winglet blades.

in the Z1, Z2, and Z3 regions. Four types of blades exhibited a larger low-pressure area on the suction surface. Meanwhile, the high pressure area appeared in the pressure surface of the blade,high pressure at the airflow deposition more,airflow from the pressure surface to the suction surface, and the leakage flow was formed. It could also be seen that Ori blades in Z1, Z2 and Z3 regions relative to SSW, PSW and TSW blades to produce negative pressure value were larger, and there was,a wider range of low pressure region. Among them, SSW blade could effectively suppress the negative pressure in the Z1 region fluctuation range and its propagation in the circumferential direction, PSW blade could effectively suppress the negative pressure in the Z2 and Z3 region fluctuation range and its propagation in the circumferential direction,while TSW blade in the three regions was mainly reflected in the suppression of high pressure region.

To investigate the full differential pressure at the blade tip, the percentage of leaf height for Z1 to Z3 was redefined, as illustrated in Fig. 7.

The total differential pressure equation is as follows.

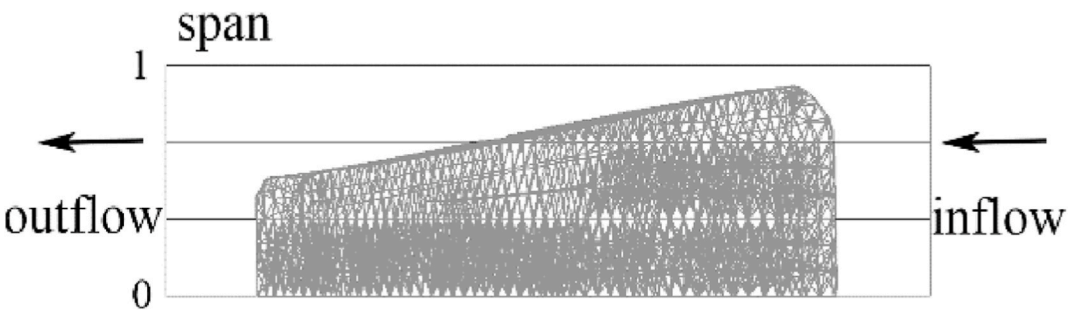

Fig. 7. Leaf apex leaf height definition.

$$\Delta p = P_{out-z} - P_{in-z} \tag{3}$$

where, Δp is the total pressure difference; P_{in-z}, the regional inlet pressure; and P_{out-z}, the regional outlet total pressure.

Fig. 8 is the comparative chart of the total pressure difference at the fan's inlet and outlet in the Z1, Z2, and Z3 regions for different blade tip winglets. For all four types of blades, the total pressure difference increased with the rise in blade height within the 90% to 100% range. It can be seen that due to the reduction of the blade tip leakage flow, there appeared a large deficit in the SSW blade and the PSW blade in the overall leaf height relative to Ori blade, leading to the export full pressure reduction. Ori blades presented significant losses relative to TSW blades at 45%–66% of blade height in the Z1 and Z2 regions of the blade tip. At low blade heights, the total pressure difference of TSW blades increased.

To quantitatively compare the blade tip blockage of different fans, the definition of blade tip blockage proposed in the literature [11,12] was applied, and the boundary of the loss area was determined through the threshold judgment of the dense flow gradient. The blockage area was then calculated by integrating the loss area, using a method similar to the definition of boundary layer displacement. The dimensionless dense flow gradient judgment criterion is as follows.

$$C_n = \left|\nabla_r\left[\frac{\rho v_l}{\rho_{ct} v_{ct}/c_{tip}}\right]\right| + \left|\nabla_\omega\left[\frac{\rho v_l}{\rho_{ct} v_{ct}/c_{tip}}\right]\right| \geq \delta \tag{4}$$

Where, ρ and v_l, are the local spatial point density and flow direction velocity; ρ_{ct} and v_{ct} , are the measurement field blade tip characterization density and velocity; c_{tip}, is the blade tip chord length; and δ, is the loss zone judgment threshold. The axial flow fan flow was low Mach number, so the effect of density was not considered and the simplified equation could be expressed as:

$$C_n = \left|\nabla_r\left[\frac{v_l}{v_{ct}/c_{tip}}\right]\right| + \left|\nabla_\omega\left[\frac{v_l}{v_{ct}/c_{tip}}\right]\right| \geq \delta \tag{5}$$

Based on the calculations for the unsteady flow field, the discriminant criterion can be used to clearly distinguish between the mainstream region and the loss region. The maximum value of Cn in the mainstream region is set as the threshold value, and any region exceeding this maximum threshold is identified as the loss region.

Fig. 9 shows the distribution of dimensionless dense flow gradient coefficients for different blade tip winglet in the axial Y = 3 mm plane. Four types of blades exhibited blockage at the blade tip, fan casing wall surface, blade wall surface, and the trailing edge part of the blade pressure surface. The blockage at the pressure surface trailing edge resulted from the large tilt of the blade installation angle, causing the inlet flow to accumulate at the blade trailing edge. Compared to the Ori blade, the TSW, SSW, and PSW blades showed a significant reduction in the range and amplitude of blade tip blockage. Additionally, the thickness of the blockage on the pressure surface wall became thinner, and the length of the pressure surface blockage got shorter. Among them, the TSW blades were the most effective in reducing the blade tip blockage, and the PSW blades significantly shortened the length of the pressure surface blockage.

After judging the loss area by δ, the blockage area was integrated in the loss area, and the dimensionless blockage coefficient b was obtained using the cross-sectional area.

$$b = \frac{\iint\left(1 - \frac{\rho v_l}{\rho_s v_s}\right)\mathrm{dA}}{A_S} \tag{6}$$

where, ρ_s and v_s are the density and velocity on the loss boundary,respectively, and A_S is the rotor denotes exit area.

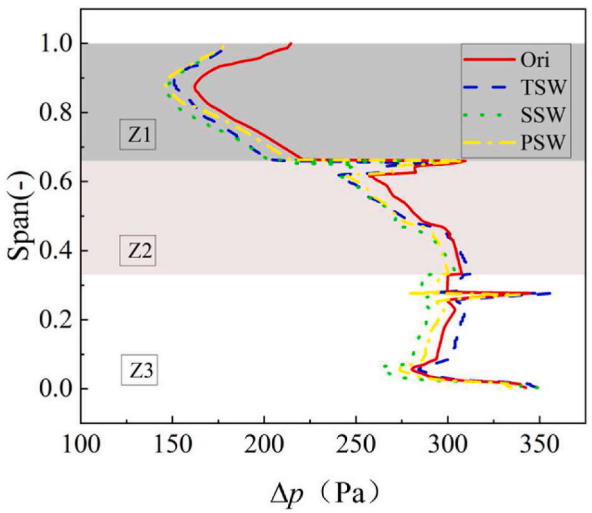

Fig. 8. Total pressure difference in the Z1, Z2 and Z3 regions for fans with different blade tip winglet.

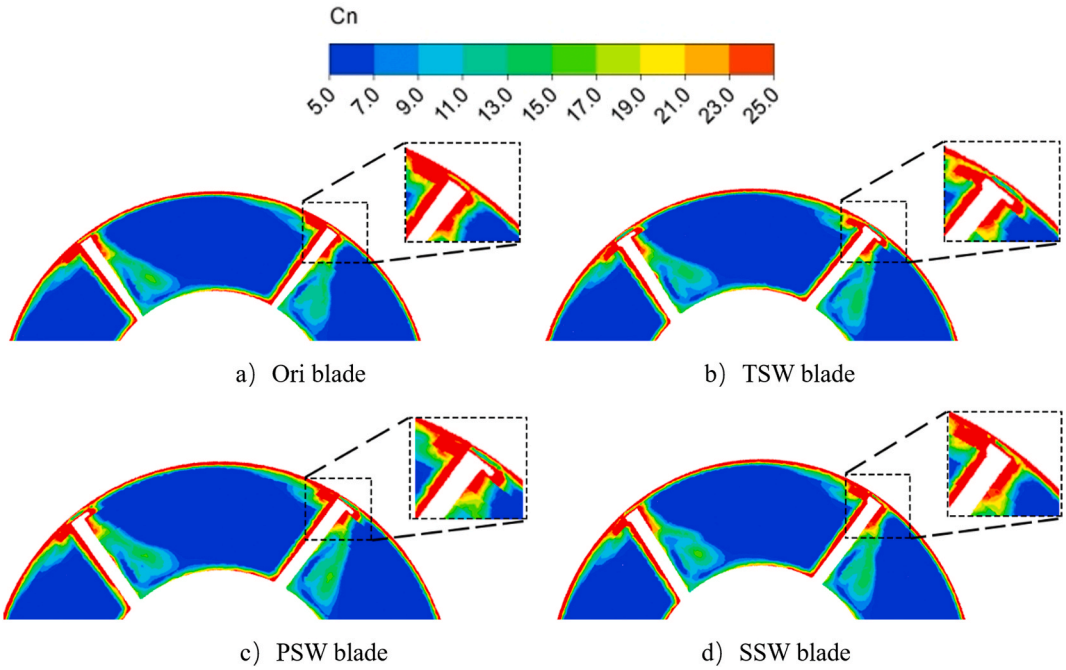

Fig. 9. Distribution of clogging coefficient of different blades.

Fig. 10 presents a schematic diagram of the loss zone at the axial plane of Y = 3 mm for the prototype fan.

Fig. 11 displays the unsteady state chordwise blockage coefficients for different blade tip winglets. It should be noted that only the effect of the blade tip winglet on the leakage flow at the blade tip was examined in this study, so that the integration was confined to the area, where the blade tip winglet was included in Z1 and Z2. By observing the blockage coefficients of different cross-sections along the flow direction, it was evidently observed that in the distal zone of the blade tip, the blockage degree of the four types of blades did not vary significantly and increased as the blade tip approached the fan casing wall. In the area approaching the blade tip, the blockage could be effectively mitigated by adding a blade tip winglet. Among them, the TSW blade exhibited the lowest blockage intensity, followed by the SSW blade.

The turbulent kinetic energy clouds of different blade tip winglet are shown in Fig. 12. In the Z1 region, Ori blades presented more thrust flow energy of fan casing wall attached flow than TSW blades and PSW. These fan casing wall attached flow was generated by the blade tip to produce larger flow velocity and fan casing impact with each other, and wide frequency noise was produced. Meanwhile, TSW blades and SSW blades reduced the turbulent kinetic energy of the tip between high flow velocity on the left side to make it homogeneous. In the Z2 region, TSW blade and SSW blade in the suction surface to produced leakage flow separation,which indicated that the suction surface to add the tip winglet could inhibit the suction surface boundary layer turbulent kinetic energy contact, and produced certain shear effect. In the Z3 region, TSW blades, PSW blades and SSW blades, at the trailing edge tip portion of the blades,homogenized their turbulent kinetic energy to different degrees.

To quantify the characteristics of the blade tip leakage flow with the addition of blade tip winglet at different faces under the same conditions, the axial momentum distribution of the blade tip leakage flow from literature [13] was applied to characterize the leakage vortex intensity at the top gap of the blade.

$$\mu = \int_{r_{tip}}^{r_{casing}} \frac{\rho V_n V_Y / \cos\alpha}{\dot{m}_{out} V_{Yin} / c_{tip}} \mathrm{d}r \tag{7}$$

where, V_n is the velocity of the blade tip leakage vortex perpendicular to the suction surface; V_Y, is the velocity of the blade tip leakage

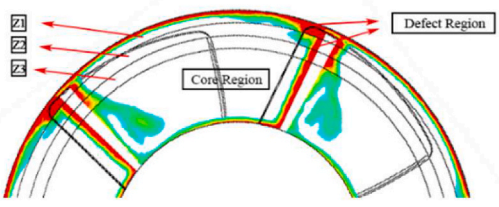

Fig. 10. Schematic diagram of the main flow area and the loss area.

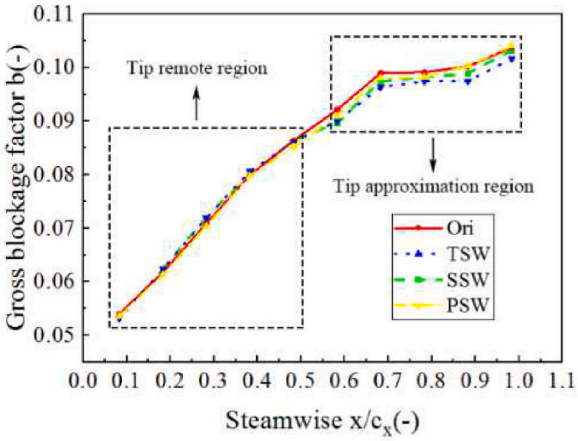

Fig. 11. Chordwise blockage coefficient of different blade tip winglets.

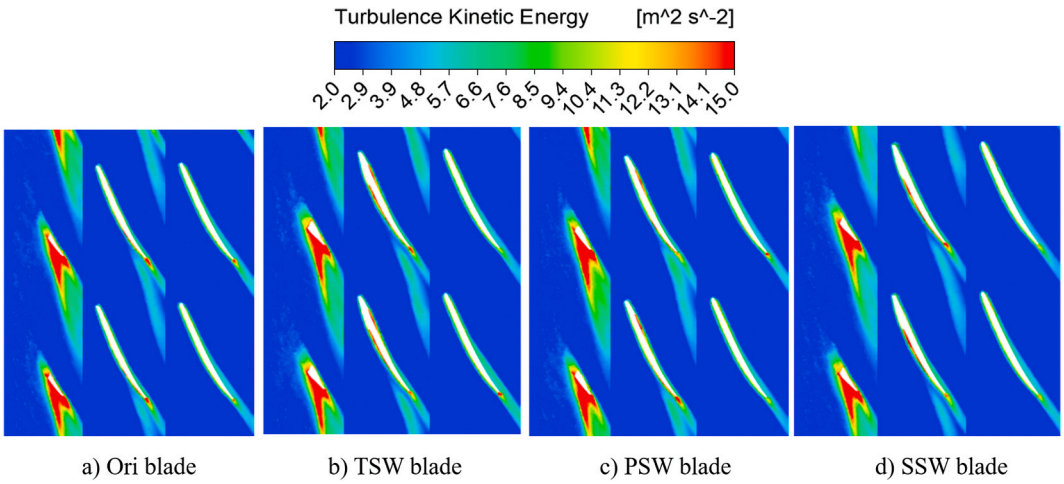

Fig. 12. Turbulent kinetic energy cloud of different blades.

vortex in the Y direction; α, is the local radian angle; and $\dot{m}_{out}$ and V_{Yin}, are the blade tip channel outlet mass flow rate and axial velocity,respectively.

The axial momentum of different blade tip winglet is shown in Fig. 13. A larger absolute value of the negative value of axial momentum indicated a stronger blade tip leakage flow against the main stream. The dimensionless peak momentum of the Ori blade was −0.164, while that of TSW, SSW and PSW blades was −0.159,−0.157 and −0.154 respectively,weaker than the blade tip leakage

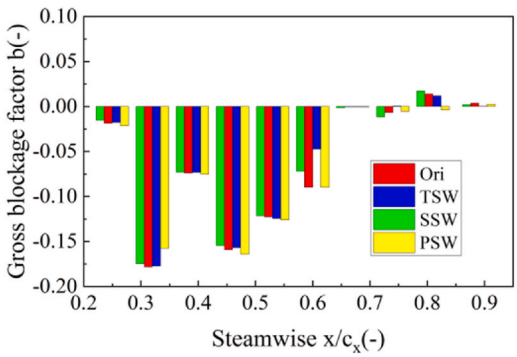

Fig. 13. Axial momentum in the chord direction for different blade tip winglets.

flow of the Ori blade against the main stream. Besides, at the sub-peak, TSW and SSW presented the same performance. At 60% of the chord length TSW and SSW blades were effective in reducing the fluctuations caused by leakage flow, while at 65% to 95% chord length, all 4 types of blades were in the low leakage flow fluctuation zone.

Subsequently to further compare the non-constant flow of different blades, four types of vortices with non-constant fields were analyzed, and the Z1, Z2, and Z3 regions in the channel were visualized using the Q-criterion, with the color mapping of the cloud diagram employing the dimensionless relative helicity to represent the direction of vortex core rotation. The angle between the absolute vortex direction and the relative velocity direction could be expressed as follows:

$$H_r = \frac{U \cdot \omega}{|U| \cdot |\omega|} \tag{8}$$

where, U is the relative velocity vector, and ω denotes the absolute vortex vector. If the two vectors have the same direction,then $H_r = 1$ and vice versa.

The structure of the $100000s^{-2}$ non-fixed-field vortex in the Q-criteria equivalent surface for the top of the different blades overall and for the different regions from Z1 to Z3 is given in Fig. 14. The overall region was first observed, and it was found that the vortex moved spirally along the airflow direction to the next blade. In the Z1 region,TSW, SSW and PSW blades in the box the relative spiral of the blade tip leakage flow for positive values significantly decreased,indicating that the addition of blade tip winglet could effectively inhibit the blade tip leakage flow along the flow direction to the next blade; in the black circle, due to the impact of the airflow generated by the negative value of the spiral impact vortex, TSW and SSW blades in the Z1 region in the fan casing wall were significantly less. In the Z2 region, it could be observed that Ori and PSW blades were more likely to produce isotropic vortices at the leading edge of the blade, and at the same time, more separating and shedding vortices were produced at the trailing edge of the blade; TSW and SSW suppressed the formation of twisting vortices at the suction side in the Z2 region as well as that of more separating and shedding vortices at the trailing edge of the blade in the Z3 region. Besides, the vortices with smaller arcs formed at the pressure side. The smaller curved vortex formed at the pressure surface increased the vortex's ability to adhere to the pressure surface to a certain extent and controlled the formation of the separation vortex.

3.2. Aerodynamic noise analysis

As depicted in Fig. 15, the addition of blade tip winglet can effectively reduce the fan aerodynamic noise, in which, SSW blade in the overall regions of Z1, Z2 and Z3 achieved a better noise reduction effect,relative to Ori blade, which reduced by 2.16 dB, 1.68 dB, 2.24 dB and 3.74 dB, respectively. In Z2 and Z3 regions, TSW blade relative to Ori blade reduced by 0.25 dB,1.51 dB and 1.02 dB respectively, but increased by 0.92 dB in the Z1 region. The PSW blade reduced by 0.27 dB, 1.38 dB and 0.56 dB in Z2 and Z3 regions, respectively, and increased by 0.55 dB in the Z1 region, relative to Ori blade. However, adding blade tip winglet on the pressure side somewhat weakened the improvement effect brought by the addition of blade tip winglet on the suction side.

Fig. 16 illustrates the sound pressure level spectrogram of the TSW blade, SSW blade and PSW blade compared with the Ori blade, where it could be observed that the addition of the blade tip winglet could produce a suppression effect on the axial flow fan aerodynamic noise at 700Hz fundamental frequency and 1400Hz octave noise that determined the sound pressure level of the axial flow fan. At the same time, the blade tip leakage vortex presented a clear broad frequency characteristic. TSW blade, SSW blade and PSW blade exhibited a comparable sound pressure level with Ori blade at frequencies of 1111Hz and 1687Hz.

In order to clearly reflect the fan noise source level,Fig. 17 shows the 1/3 frequency range diagram of sound pressure level A of different blades, where it could be found that the main noise output of the axial flow fan was in the low frequency region. In most frequency bands, the noise of TSW blade, SSW blade and PSW blade was significantly reduced, while the frequency band of 630Hz–800Hz, the noise of TSW blade, SSW blade and PSW blade was 4.61 dB,8.13 dB and 5.35 dB lower than that of Ori blade, respectively, and in the frequency band of 800 Hz–3150 Hz, the maximum noise level of TSW blade and PSW blade increased by 2.05 dB and 2.15 dB compared with Ori blade, while that of SSW blade decreased by 0.90 dB. At the medium frequency 3150Hz–5000Hz, the noise level followed the order of Ori blade > TSW blade > SSW blade > PSW blade. In the middle and high frequency range of 5000Hz–6300Hz, the noise level was PSW blade > Ori blade > TSW blade > SSW blade. SSW blades and PSW blades were provided with more noise reduction properties at high frequency of 6300Hz–10000 Hz.

4. Conclusion

Herein, the effect of different blade tip winglet add-on surface schemes on the internal flow characteristics and acoustic performance of the axial flow fan blade tip was investigated by numerical simulation combined with experimental verification of the blade tip partition. The main conclusions are as follows.

(1) SSW, PSW and TSW blades could effectively control the generation of low pressure area, SSW blades control range in Z1 rigion as well as PSW blades control orientation in Z2 and Z3 rigion, and had different degrees of full differential pressure loss at different partitions of the blade tip.
(2) The addition of blade tip winglet could effectively improve the blade tip Z1 rigion and Z2 rigion blockage, of which TSW blade presented the best effect; TSW, SSW, PSW blades could effectively reduce the Z1 rigion fan casing wall attached flow turbulence

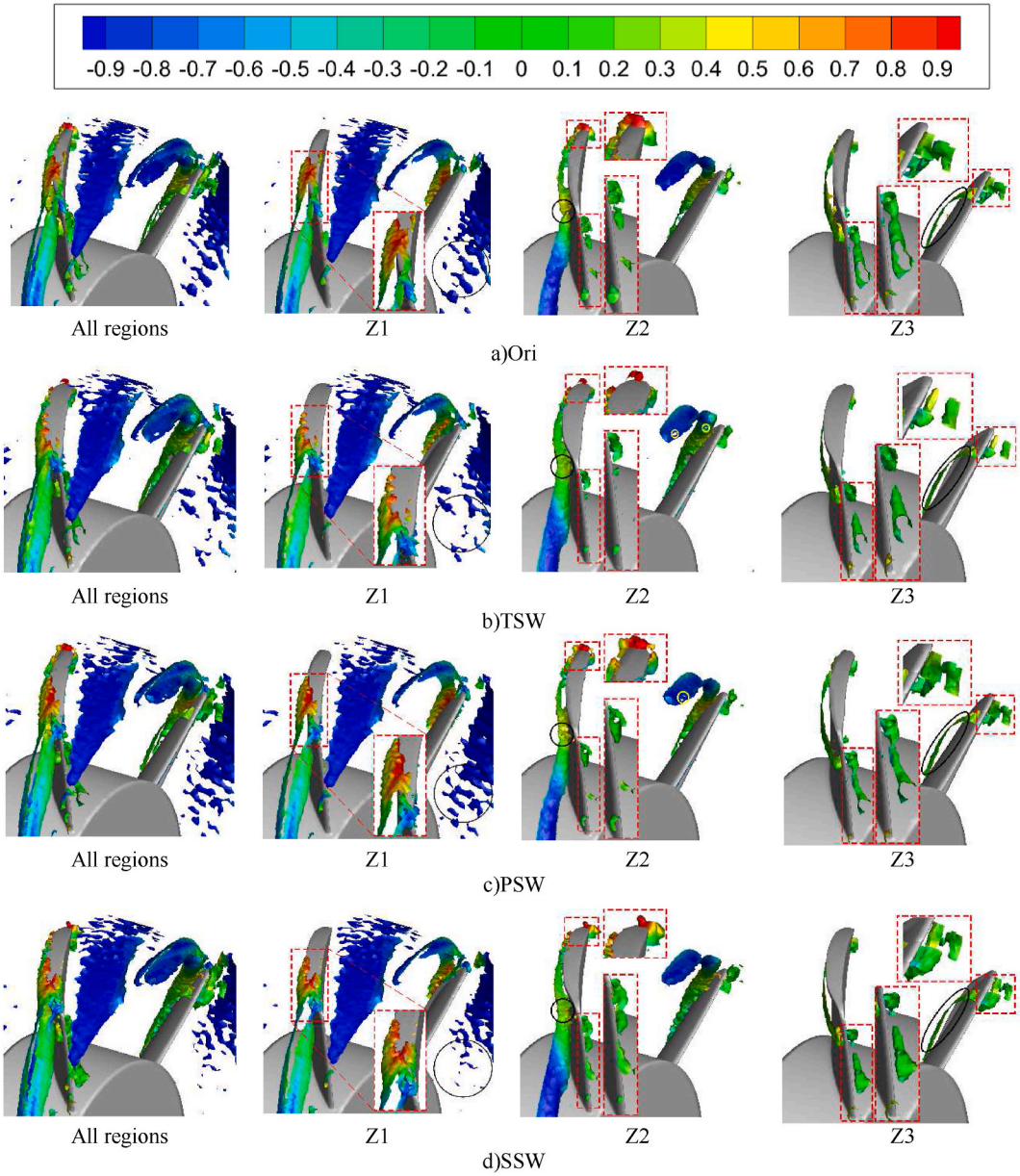

Fig. 14. Distribution of the vortex nuclei structure in Z1, Z2 and Z3 regions for different blades.

energy, suppress the broadband noise; TSW, SSW and PSW blades also effectively reduced the leakage flow and the mainstream of the confrontation ability, with TSW and SSW blades presenting a better effect at 60% chord length.

(3) TSW, SSW and PSW blades in the Z1 rigion could effectively inhibit the blade tip leakage flow positive flow to the next blade, reduce the helicity for the negative value of the impact vortex; Ori and PSW blades in Z2 rigion were more likely to produce isotropic vortex in the leading edge of the blades, while TSW and SSW blades could slow down the pressure surface attached vortex detachment in the Z3 rigion.

(4) Adding blade tip winglet mainly reduced discrete noise at the reference and octave frequencies,thus achieving effective reduction of the total sound pressure level of the axial flow fan; TSW, SSW and PSW blades mainly reduced noise in the low frequency band, and SSW blades presented better noise reduction properties in the total sound pressure level and each frequency band.

Funding

2022 annual central guidance for local science and technology development funds (Qianzhongyindi [2022] 4007).

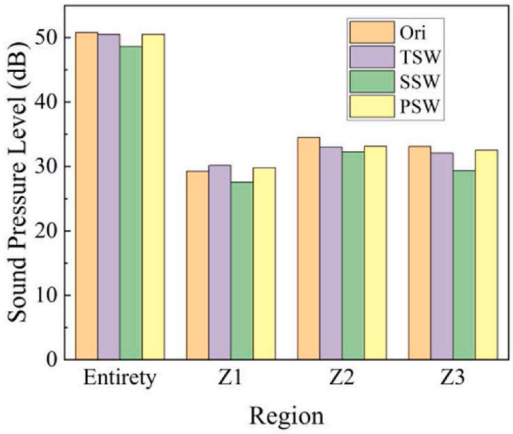

Fig. 15. Total sound pressure level in different areas with different blades.

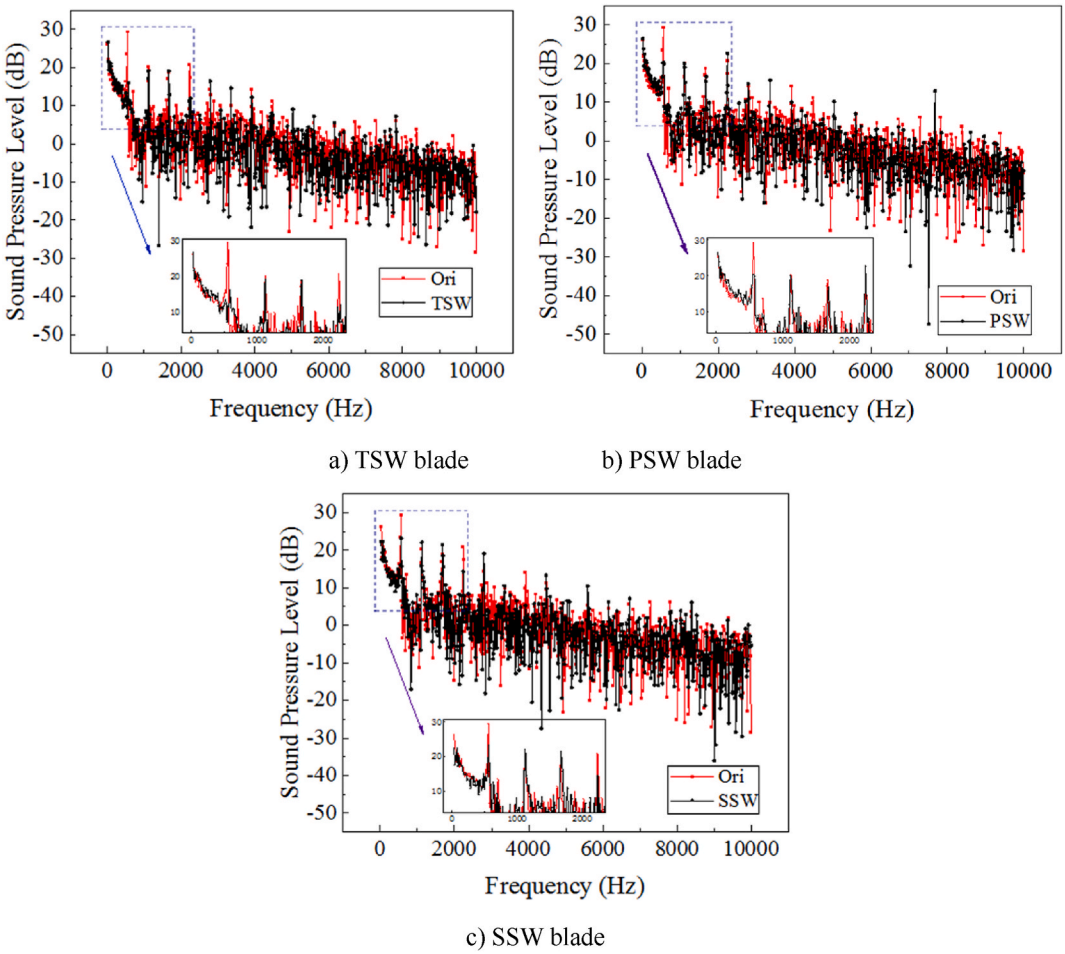

Fig. 16. Comparison of sound pressure level spectrum of different winglet blades and Ori blades.

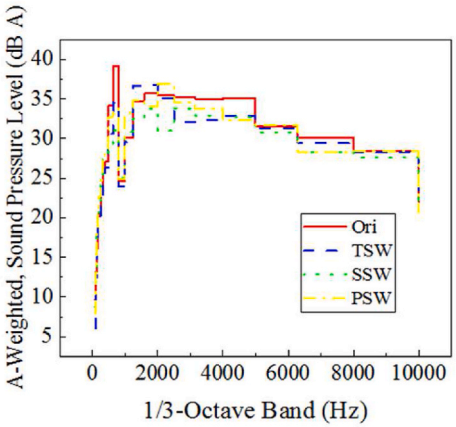

Fig. 17. 1/3 Octave band diagram of sound pressure level of fans with different blade tip winglet.

Code or data availability

Not applicable.

Ethics approval

Not applicable.

Consent to participate

All authors have read and agreed to the published version of the manuscript.

Author contribution statement

Lei Diao: Conceived and designed the experiments; Performed the experiments; Analyzed and interpreted the data; Contributed reagents, materials, analysis tools or data; Wrote the paper.

Fahua Ge: Performed the experiments.

Yong Liu: Analyzed and interpreted the data.

Lin Yang; Youen Liu; Qi Huang: Contributed reagents, materials, analysis tools or data.

Data availability statement

The data that has been used is confidential.

Declaration of competing interest

The authors declare that they have no known competing financial interests or personal relationships that could have appeared to influence the work reported in this paper.

Acknowledgments

The authors would like to thank Professor Meng Tao from the School of Mechanical Engineering,Guizhou University for his valuable comments. Thanks for the support of 2022 annual central guidance for local science and technology development funds (Qianzhongyindi [2022] 4007) Fund.

References

Periodicals

[1] Maaloum,A.,Kouidri,S.,& Rey,R.Aeroacoustic performance evaluation of axial flow fans based on the unsteady pressure field on the blade surface. Appl. Acoust.,65(4),367–384 doi:10.1016/j.apacoust.2003.10.004.

[2] Jung,J.H.,& Joo,W. Effect of tip clearance,winglets,and shroud height on the tip leakage in axial flow fans. Int. J. Refrig. doi10.1016/J.IJREFRIG.2018.07.010.

[3] M. Hoeger, Lahmer, et al., A correlation for tip leakage blockage in compressor blade passages, J. Turbomach. 122 (3) (2000) 426, https://doi.org/10.1115/1.1303707, 426.

[4] B.J. Liu, Z.B. Zhang, X.J. Yu, Experimental investion on characteristics of tip leakage in an axial compressor, Acta Aeronautica et Aeronautica Sinica 34 (12) (2013) 2682–2691, https://doi.org/10.7527/S1000-6893.2013.0181.
[5] S. Han, J. Zhong, H. Lu, et al., Effect of winglet geometry arrangement and incidence on tip clearance control in a compressor cascade, J. Therm. Sci. 23 (2014) 381–390.
[6] Bizjan,B.,Milavec,M.,Širok,B.,Trenc,F.,& Hočevar,M. Energy dissipation in the blade tip region of an axial fan. J. Sound Vib.,382,63–72. doi:10.1016/j.jsv.2016.06.036.
[7] E. Schneehagen, T.F. Geyer, E. Sarradj, et al., Aeroacoustic noise reduction by application of end plates on wall-mounted finite airfoils, Exp. Fluid 62 (2021) 106, https://doi.org/10.1007/s00348-021-03204-9.
[8] A. Nashimoto, N. Fujisawa, T. Akuto, et al., Measurements of aerodynamic noise and wake flow field in a cooling fan with winglets, J. Vis. 7 (2004) 85–92, https://doi.org/10.1007/BF03181488.
[9] M. Milavec, B. Širok, D. Vidal de Ventos, et al., Identification of noise generation and flow kinematics in the air gap for two different blade tip designs of an axial fan, Forsch Ingenieurwes 79 (2015) 29–39, https://doi.org/10.1007/s10010-015-0185-2.
[10] Wei Yang, Yafan Duan, Xueqing Dong, et al., Effect of tip winglet with airfoil on tip surface velocity, Acta Energlae Solaris Sinica 42 (11) (2021) 260–264, https://doi.org/10.19912/j.0254-0096.tynxb.2019-1199.
[11] S.A. Khalid, The Effects of Tip Clearance on Axial Compressor Pressure Rise[D], Massachusetts Institute of Technology, 1995.
[12] S.A. Khalid, A.S. Khalsa, I.A. Waitz, et al., Endwall blockage in axial compressors, J. Turbomach. 121 (3) (1999) 499–509.
[13] M. Hewkin-Smith, G. Pullan, S. Grimshaw, et al., The Role of Tip Leakage Flow in Spike-type Rotating Stall Inception[C], 2017. ASME Paper No. GT2017-63655.